Check for updates

Simulating open quantum systems with molecular spin qudits†

Sebastián Roca-Jerat, [ID] [ae] Emilio Macaluso, [ID] [b] Alessandro Chiesa, [ID] [bcd] Paolo Santini [ID] [bcd] and Stefano Carretta [ID] *[bcd]

Noise affecting quantum processors still limits quantum simulations to a small number of units and operations. This is especially true for the simulation of open quantum systems, which involve additional units and operations to map environmental degrees of freedom. Hence, finding efficient approaches for the simulation of open quantum systems is an open issue. In this work, we demonstrate how using units with $d > 2$ levels (qudits) results in a reduction of up to two orders of magnitude in the number of operations (gates) required to implement state-of-the-art algorithms. We explore two conceptually distinct families of these algorithms that were initially designed for qubits and discuss the gate complexity scaling that different platforms (qubit-based *vs.* qudit-based) offer. Additionally, we present realistic simulations of an experimental platform based on molecular spin qudits coupled to superconducting resonators, where the main hardware error sources are included. We show that, in all cases considered, the use of qudits leads to a remarkable reduction in circuit complexity and that molecular nanomagnets are ideal qudit hosts.

New concepts

We propose a new point of view about the digital quantum simulation of open quantum systems (OQS) by showcasing the potential of units with more than two logical levels (qudits). Efficiently simulating OQS is important for designing novel quantum technologies. We demonstrate that qudits reduce the number of gates needed for incoherent (but controlled) dynamics by nearly two orders of magnitude using state-of-the-art algorithms originally conceived for qubits. This improvement helps to bridge the gap between circuit execution times and decoherence times in current noisy devices. We show that molecular nanomagnets coupled to superconducting resonators are ideal materials to implement this novel approach to quantum simulations, exploiting the chemical tunability of molecular spin qudits combined with the ability of superconducting resonators to wire and control them. This work opens the door for an efficient use of molecular qudits to circumvent the poor scaling in the number of non-local gates required to simulate OQS exhibited thus far by qubit-based platforms and promotes the synthesis of new molecular materials designed to provide the required number of levels and optimal connectivity for faster circuit execution.

1 Introduction

The ever-growing development of quantum computers recently allowed for public accessibility to noisy intermediate-scale

[a] Instituto de Nanociencia y Materiales de Aragón (INMA), CSIC-Universidad de Zaragoza, Zaragoza 50009, Spain

[b] Università di Parma, Dipartimento di Scienze Matematiche, Fisiche e Informatiche, 43124 Parma, Italy. E-mail: stefano.carretta@unipr.it

[c] Gruppo Collegato di Parma, INFN-Sezione Milano-Bicocca, I-43124 Parma, Italy

[d] UdR Parma, INSTM, I-43124 Parma, Italy

[e] Departamento de Física de la Materia Condensada, Universidad de Zaragoza, Zaragoza 50009, Spain

† Electronic supplementary information (ESI) available: Details on the numerical simulations, on both algorithms (with circuit decompositions into qubit-based and qudit-based platforms of the dynamical map into elementary one- and two-qudit gates and their implementation on the molecular spin quantum hardware), and on the simulation of an open system of two qubits (super-operator formalism and entangling gates mediated by the resonator). See DOI: https://doi.org/10.1039/d4mh01512f

quantum (NISQ) computers.[1] Now, great efforts of conceptualization and implementation of efficient quantum simulations is bringing closer the future envisioned by Feynman[2] in which we are finally able to tackle quantum phenomena which go beyond classical computation.[3] However, interaction with the environment typical of open quantum systems (OQS) represents a double-edged sword in such applications. On the one hand, it is the primary cause of the "noisy" nature of nowadays quantum simulators, limiting the computational power of algorithms developed on such platforms. On the other hand, since most quantum systems of relevant interest are effectively OQS, quantum simulators are faced with the problem of simulating non-unitary time evolution together with the coherent Hamiltonian dynamics. This represents a significant challenge, since in the digital computing paradigm the controlled dynamics simulated by quantum computers is limited to unitary quantum gates. This challenge has been met with considerable theoretical developments over the last two decades,[4–15] resulting in initial experimental demonstrations

on multiple qubit-based systems.[16–23] In all these algorithms, an auxiliary system, or ancilla, serves as an artificial environment with which the target system interacts. We distinguish two main families of techniques. The first comprises algorithms based on Stinespring's dilation theorem,[24] where the dimension of the ancilla system increases with the complexity of the environment being simulated,[7,10,19,21,23,25] offering a more straightforward implementation at the cost of a larger ancilla system. The second calls for usually more sophisticated circuits but maintains the advantage of a small and constant ancilla register dimension regardless of problem size.[6,8,18,22,26–31]

In this work, we demonstrate how the use of units with $d > 2$ levels (qudits) can significantly decrease the circuit complexity for both classes of algorithms. The use of qudits to simulate OQS was already proposed in ref. 32 to encode the degrees of freedom of the system, but not for the environment. Here, we show a more general study on how the use of qudits can be crucial for hosting both the target system and the ancilla in a wide variety of scenarios. We present a detailed implementation proposal for simulating OQS on a real platform based entirely on molecular spin qudits.[33,34] These systems exhibit promising features for quantum computing, including long coherence times even at high temperatures[35–39] and efficient implementation of single- and multi-qubit gates *via* microwave or radio-frequency pulses.[40,41] The high degree of chemical control over their synthesis allows tailoring energy levels for specific applications[42,43] and limiting decoherence.[35,44] This chemical engineerability facilitates scalability of multi-qubit systems with switchable interactions, achievable through molecular spins alone[34,42,43] or by integrating them with superconducting resonators.[45–49] Importantly, molecular spin qudits—derived from individual spin $S > 1/2$ ions or low-energy multiplets of strongly coupled magnetic ions—can reduce the number of computational units and required gates for a given algorithm, potentially offering computational bases more resilient to decoherence.[34] The versatility offered by molecular systems can benefit other applications such as quantum error correction[50–52] and quantum simulation of closed systems.[43,53,54]

Here, we demonstrate that molecular spin qudits also provide an efficient platform for simulating OQS. For both families of algorithms mentioned above, we demonstrate a remarkable reduction of circuit complexity (up to two orders of magnitude) by replacing multiple qubits with $d > 2$ qudits. Specifically, complexity is measured by the number of required single- and two-body gates.[55,56] This reduction is especially pronounced when the target of the simulation involves multi-level systems (*e.g.* spins $S > 1/2$). We perform numerical simulations for the combined coherent and incoherent dynamics of target one- and two-qubit systems, using both algorithms, finding very good results. These simulations are based on the blueprint of a molecular-spin quantum processor consisting of molecular spin qudits strongly coupled to superconducting resonators[45] and include the most significant errors related to dissipation and decoherence. These results open the door for the integration of qudits into quantum digital computation, enabling the efficient tackling of complex problems where the use of qubits is inefficient.

2 Results

2.1 Qubits *vs.* qudits for simulating open quantum systems

We start by taking as a practical example a spin-3/2 particle interacting with a Markovian bath. The dynamics of such an OQS can be described by the Lindblad equation:

$$\dot{\rho}(t) = -\frac{i}{\hbar}[\mathscr{H}, \rho(t)] + \sum_k \left(2L_k\rho(t)L_k^\dagger - L_k^\dagger L_k\rho(t) - \rho(t)L_k^\dagger L_k \right),$$

$$(1)$$

where H and L_k are the Hamiltonian and jump operators, describing the coherent and incoherent dynamics of the system, respectively, and $\rho(t)$ is the system density matrix at time t. If both $\mathscr{H}$ and L_k do not depend explicitly on time, eqn (1) can be directly integrated as $|\rho(t)\rangle = \mathrm{e}^{\mathscr{L}t}|\rho(t = 0)\rangle$, where $|\rho\rangle$ is the unraveled density operator in the vector form and $\mathscr{L}$ is the related super-operator.[57] The Lindblad equation relies on the Born (weak system–bath interaction), Markov (no memory of the bath) and secular approximations.[58,59] Some of the above assumptions can fail in describing decoherence in relatively small molecules. For instance, the Markov approximation is not fulfilled where the nuclear spin bath is of limited size. Nonetheless, the Lindblad description represents one of the simplest and most widely used formalisms to model decoherence and hence is an optimal starting point for investigating algorithms on the quantum simulation of open systems. We also note that the presented approaches could be extended also to more complex forms of the system–bath interaction, which are not captured by the Lindblad formalism.

The evolution given by $M(t) = \mathrm{e}^{\mathscr{L}t}$ commonly consists of several non-commuting terms which are implemented through a series of subsequent unitary gates on the hardware. For instance, one could split $\mathscr{L}$ into the coherent and incoherent dynamics, $\mathscr{L} = \mathscr{L}_c + \mathscr{L}_{inc}$. The Suzuki–Trotter approximation allows for a simple solution to this problem by replacing the time-evolution operator $M(t) = \mathrm{e}^{\mathscr{L}t}$ with multiple operators $M_i(t/N_T) = \mathrm{e}^{\mathscr{L}_i t/N_T}$ which can all be translated into quantum gates. This can be written as:

$$M(t) = \mathrm{e}^{\sum_i \mathscr{L}_i t} \approx \left(\prod_i \mathrm{e}^{\mathscr{L}_i \Delta t} \right)^{N_T}, \qquad (2)$$

where $\mathscr{L}_i$ are non-commuting terms of $\mathscr{L} = \sum_i \mathscr{L}_i$, $\Delta t = t/N_T$ and N_T is the number of Trotter steps. The larger the N_T, the smaller the error introduced by this approximation (a.k.a. digital error), which scales as $\mathcal{O}(t^2/N_T^2)$.[60] However, in NISQ devices each gate involves an error (due, *e.g.*, to decoherence or imperfections in the implementation) and hence increasing N_T yields a detrimental error accumulation. The choice of N_T is therefore associated to a trade-off between digital and implementation errors. For a more comprehensive discussion on the possible errors one may encounter in NISQ devices, we refer the reader to ref. 23.

Alternatively, the dynamics of the OQS can be computed at discrete time steps through the dynamical map:

$$\rho(t) \equiv \mathscr{E}[\rho(0)] = \sum_{k=1}^{r} E_k \rho(0) E_k^{\dagger}, \qquad (3)$$

where E_k are the Kraus operators at time t, satisfying the condition $\sum_k E_k^{\dagger} E_k = \mathscr{I}$, and r is the Kraus rank or Choi rank, such that $r \leq d_s^2$, d_s being the dimension of the Hilbert space. This description is usually employed by algorithms in which the ancilla mimics the environment, and its effect on the target system is divided into the successive application of the different operators E_k.[19]

The first algorithm we consider belongs to this family of algorithms, in which two registers are required. The first one contains the degrees of freedom of the target system (for instance, the spin-3/2 with $d_s = 4$). The second one is an ancilla which mimics the environment and whose size grows with the rank of the Kraus map in eqn (3). The joint coherent and incoherent evolution (driven, respectively, by $U_{\mathscr{H}}(\Delta t) = \exp[-i\mathscr{H}\Delta t]$ and by eqn (3)) can be implemented by exploiting a Suzuki–Trotter decomposition [eqn (2)] of the associated super-operator. The quantum circuit accomplishing this is presented in Fig. 1(b). On the left side, the circuit originally proposed for qubits is shown. Two qubits are needed to represent the target spin-3/2 system, and up to 4 qubits as the ancilla to represent the most general scenario, where the Kraus rank is maximum, $r = d_s^2 = 16$. The block labeled $e^{\mathscr{L}_{inc}\Delta t}$ represents the interaction between the environment and the spin-3/2 system. The set of Kraus operators is represented in a basis of unitary operations,

$\{U_i\}_{i=0,15}$, such as the Pauli matrices, which are the conditional operations applied to the target system. The weights corresponding to each Kraus operator are encoded in the V and W operations, fulfilling the condition $E_k = \sum_{i=0}^{r} W_{ki} V_{i0} U_i$. Finally, a projective measurement on the ancilla traces out the environment's degrees of freedom, effectively applying the incoherent channel over the target system.

The number of single- and two-qubit gates required to implement the incoherent part of the dynamics is substantial, as shown in the histogram of Fig. 1(b), mainly due to the necessity of performing gates on the system qubits controlled by the state of all the environment qubits (generalized Toffoli gates; see the ESI†). These non-local operations are required to mimic the entanglement of the environment to the system and represent the main bottleneck of a qubit-based approach. This problem is effectively overcome by using a circuit composed of only two qudits, where a ququart acts as the target system and a 16-level qudit acts as an artificial bath. In this scenario, entangling gates are performed between two physical units, removing the need for non-local operations and causing a staggering reduction in gate complexity: from $\mathcal{O}(16\,000)$ gates to $\mathcal{O}(800)$. Note that this only takes into account the block corresponding to the incoherent part and a single Trotter step. Therefore, this reduction becomes even more remarkable when considering the full time evolution.

The second algorithm we consider is shown in Fig. 1(c). It is based on the implementation of the operator $M = e^{\mathscr{L}t}$ in a single block by dilating the Hilbert space with a 4-level ancilla,[27,28] regardless of the dimensionality of $\mathscr{L}$. Note that, since the
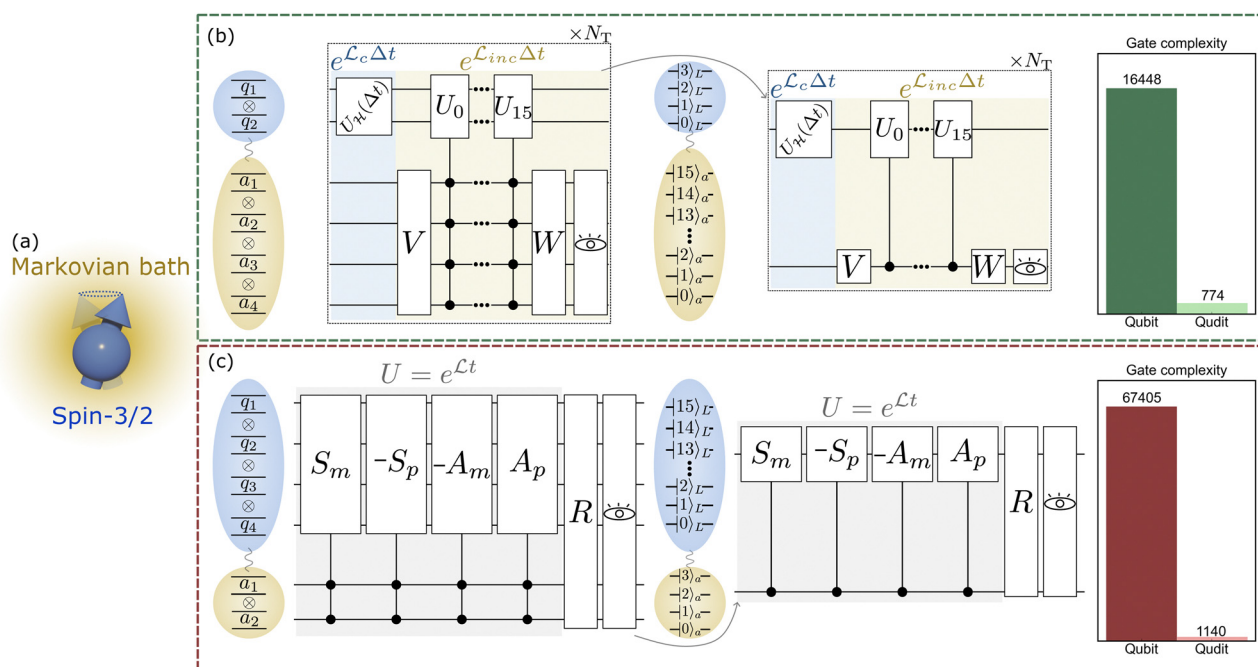

Fig. 1 Quantum simulation of the dynamics of a spin-3/2 particle coupled to a Markovian bath, schematized in (a), using two different algorithms (b) and (c). For each of these algorithms, the implementation using qubits (left circuit) and qudits (right circuit) is shown. The gate complexity associated with each circuit is represented in the histograms as the height of each bar.

super-operator M acts on the space of the vectorized density matrix, the register that stores the degrees of freedom of the target system must have d_s^2 levels. We begin by expressing this M as a sum of four unitary operators according to the following Taylor expansion:

$$M = \lim_{\varepsilon \to 0} \frac{1}{2\varepsilon}(S_m - S_p - A_m + A_p), \qquad (4)$$

where ε is the expansion parameter, $S_m = -S_p^\dagger = ie^{-i\varepsilon S}$, $A_m = A_p^\dagger = e^{-\varepsilon A}$ and S and A are, respectively, the Hermitian and anti-Hermitian components of the original operator $M = S + A$. Each unitary operator in eqn (4) is then implemented on four different subspaces all initialized as $|\rho(0)\rangle$ and subsequently their amplitudes are summed into one of these subspaces. This can be represented as

$$RU|\rho(0) \oplus \rho(0) \oplus \rho(0) \oplus \rho(0)\rangle = |\rho(t) \oplus \nu_1 \oplus \nu_2 \oplus \nu_3\rangle, \qquad (5)$$

where U contains all four unitary operators and R performs linear combinations of the four density operators, effectively summing their amplitudes into the first subspace, where $|\rho(t)\rangle$ is finally obtained. The other linear combinations ν_1, ν_2 and ν_3 on the remaining subspaces are of no physical interest. Hence, a final projective measurement to restrict to the subspace of interest is needed. Then, the operator U can be written as the $4d_s^2$-sized matrix:

$$U = \begin{pmatrix} S_m & 0 & 0 & 0 \\ 0 & -S_p & 0 & 0 \\ 0 & 0 & -A_m & 0 \\ 0 & 0 & 0 & A_p \end{pmatrix}. \qquad (6)$$

Once again, we present the circuit that implements this algorithm on both a qubit-based platform and a qudit-based platform in Fig. 1(c). Note that the dimensionality of the registers is reversed compared to the previous method [cf. Fig. 1(b)]. Now the gate complexity is even greater than before. This is because both coherent and incoherent dynamics are fully included in the operation U and the matrices S_m, S_p, A_m, and A_p have a much more complex internal structure than the matrices U_i of the previous algorithm. However, qudits enable the realization of such operations as controlled gates between two physical units, inducing an even more pronounced decrease in gate complexity with respect to the first algorithm, reaching a factor of ~ 60. All information regarding the derivation of the gate complexity in each scenario, as well as a more detailed description of each algorithm, can be found in the ESI.†

Consequently, a qudit approach not only achieves an obvious reduction in the number of physical units in the circuit, but dramatically cuts down the number of single- and two-body gates required for implementation, leading to a substantial increase in efficiency and scalability. In light of this potential, researchers using different platforms are exploring ways to extend control over their units beyond two levels. Examples include transmons,[61] trapped ions[62,63] or magnetic

molecules.[34] The latter could offer greater versatility in hosting qudits, due to their ability to accommodate and coherently control many levels, which can also offer a very high mutual connectivity. A clear example of this is the vanadyl porphyrin molecule,[64] which hosts an $S = 1/2$ electronic spin coupled to an $I = 7/2$ nuclear spin and could be a suitable candidate for the 16-level qudit proposed in Fig. 1.

2.2 Molecular nanomagnets as qudits

Having established that the use of qudits presents a remarkable advantage, we now show that these algorithms can be efficiently implemented on a platform based on molecular spin qudits. Molecular nanomagnets offer a broad catalog of qudit candidates, from complexes with electronic spin to complexes that combine them with nuclear spins, naturally more protected from interaction with the environment. Progress has been made in recent years to produce systems with longer and longer coherence times even scratching the millisecond scale.[35] Here we mention a few notable examples and refer the reader to ref. 65 for a more detailed review on the subject. The Cr₇Ni polynuclear ring with ground state $S = 1/2$ is a very good qubit candidate for its remarkable chemical tunability. In particular, Ni^{2+} can be replaced with another divalent ion (such as Mn^{2+} or Zn^{2+}), thus changing the total spin of the ground multiplet from 1/2 to 1 or 3/2 and making the resulting ring a potential qudit. In addition, engineering the ligands enabled the reduction of low-energy vibrations and the increase of the coherence time from a few μs to 15 μs.[44] Even more importantly, several rings can be combined together into complex supramolecular structures with tailored interactions[42,66,67] which can fulfill specific requirements for implementing quantum algorithms. This point is important for the scheme we propose below and will be discussed further.

Mononuclear systems based on transition metal ions are also promising qudit candidates. For instance, the $[Cr^{3+}(C_2O_4)_3]^{3-}$ (ref. 68) complex shows an electronic spin $S = 3/2$ and coherence times of a few μs.

Moreover, molecules consisting of an (effective) electronic spin 1/2 coupled by a strong hyperfine interaction with a nuclear spin $I \geq 3/2$ can encode nuclear spin qudits more robust against noise. Examples are represented by Ln-based mononuclear complexes such as Yb(trensal) ($S = 1/2$, $I = 5/2$)[69] or TbPc₂ ($I = 3/2$)[70] and by VO compounds such as VO(TPP) ($S = 1/2$, $I = 7/2$), which stands out for its remarkable coherence times of up to 64 μs. VO ions have already been combined into dimers for two-qubit gates[71,72] and have demonstrated resilience to decoherence even at high temperatures.[37]

As a first case study, we consider the case of a single spin-1/2 coupled to a depolarizing channel (DEP). This channel can be described either through the jump operators $\{L_k\}_{k=0}^2 = \{\sqrt{\gamma}S_x, \sqrt{\gamma}S_y, \sqrt{\gamma}S_z\}$, ($S_i = \sigma_i/2$ and σ_i are the Pauli matrices) with $\gamma = 1/T_{DEP}$, or by the set of Kraus operators $\{E_k\}_{k=0}^3 = \left\{\sqrt{1 - \frac{3p}{4}}\mathscr{I}, \sqrt{\frac{p}{4}}\sigma_x, \sqrt{\frac{p}{4}}\sigma_y, \sqrt{\frac{p}{4}}\sigma_z\right\}$ with $p(t) = 1 - \exp[4t/T_{DEP}]$.

This channel drives the system towards the maximally mixed state with probability $p(t)$: $\rho(t) = [1 - p(t)]\rho(0) + p(t)\mathscr{I}/2$.

We begin by applying the algorithm described in Fig. 1(b). As discussed in the previous section, we need a two-level system to act as our spin-1/2 and a ququart to incorporate the degrees of freedom of the Kraus map. The coherent part of the evolution is driven by $U_{\mathscr{H}}(\Delta t) = \mathrm{e}^{-i\mathscr{H}\Delta t}$, where $\mathscr{H} = \frac{\Omega}{2}\sigma_x$. This Hamiltonian in conjunction with the DEP channel gives rise to damped Rabi oscillations. The block of operations that implements the DEP channel, labeled as $\mathrm{e}^{\mathscr{L}_{\mathrm{inc}}\Delta t}$ in Fig. 1(b), is constructed from the decomposition of the Kraus operators into unitary operators. In this case, the process is straightforward. The controlled operations U_j correspond to the Pauli operators, $\{U_i\} = \{I, \sigma_x, \sigma_y, \sigma_z\}$, while the matrices V and W adjust the weights associated with each operator. In this case,

$$\{V_{i0}\}_{i=0}^{3} = \left\{ \sqrt{1 - \frac{3p}{4}}, \sqrt{\frac{p}{4}}, \sqrt{\frac{p}{4}}, \sqrt{\frac{p}{4}} \right\} \text{ and } W = \mathscr{I}. \text{ Note that in}$$

this algorithm the ancilla register always starts and ends in the ground state $|0\rangle_a$, so only the first column of the matrix V is of interest. The remaining columns can be completed arbitrarily as long as the unitarity condition is satisfied (for more details on the algorithm see the ESI†).

As a molecular system to implement this algorithm, we propose the complex schematized in the inset of Fig. 2(a). It consists of two spins (A,B) which encode the degrees of freedom of both the system and environment, respectively. Both are coupled to an antiferromagnetic dimer (M, $S_1^M = S_2^M = 1/2$) which provides a switch of the effective A–B interaction.[43] For the here-examined case of a single-qubit system subject to the depolarizing channel, we can choose $S_A = 1/2$ and $S_B = 3/2$. This molecular complex is described by the spin Hamiltonian ($\hbar = 1$):

$$\begin{aligned} H_{\mathrm{MOL}} &= \mu_B B_0 \left[g_z^A S_z^A + g_z^B S_z^B + g_z^M \left(S_{1z}^M + S_{2z}^M \right) \right] \\ &\quad + D_B \left(S_z^B \right)^2 + \Delta \mathbf{S}_1^M \cdot \mathbf{S}_2^M + J \sum_{\alpha=A,B} \sum_{i=1,2} \mathbf{S}_\alpha \cdot \mathbf{S}_i^M. \end{aligned} \tag{7}$$

Based on the brief review of possible candidates for spin molecular qudits at the beginning of the section, a possible realization of this architecture could be a supramolecule in which A is a Cr_7Ni ring, B is a Cr^{3+} in an approximately octahedral crystal field environment and the switch is a Cu_2 dimer, similar to what was proposed in ref. 66. In Hamiltonian (7), $g_z^A = 1.84$, $g_z^B = 1.98$, are typical gyromagnetic ratios for Cr_7Ni and Cr^{3+}, B_0 is the external magnetic field and $D_B/2\pi = 5.2$ GHz is a typical axial zero-field splitting of Cr^{3+},[73] which ensures that all qudit energy gaps are well separated in energy and hence individually addressable by microwave pulses of different frequencies. Note that the zero-field splitting anisotropy term in eqn (7) is important to make the qudit spectrum anharmonic (*i.e.* with all energy gaps different) and hence allow for a universal control of the qudit. In particular, increasing anisotropy helps to mitigate leakage problems during coherent control by faster pulse sequences. However, increasing the gap between levels too much can lead to an increase in the relaxation rates.[74] The isotropic exchange interaction within
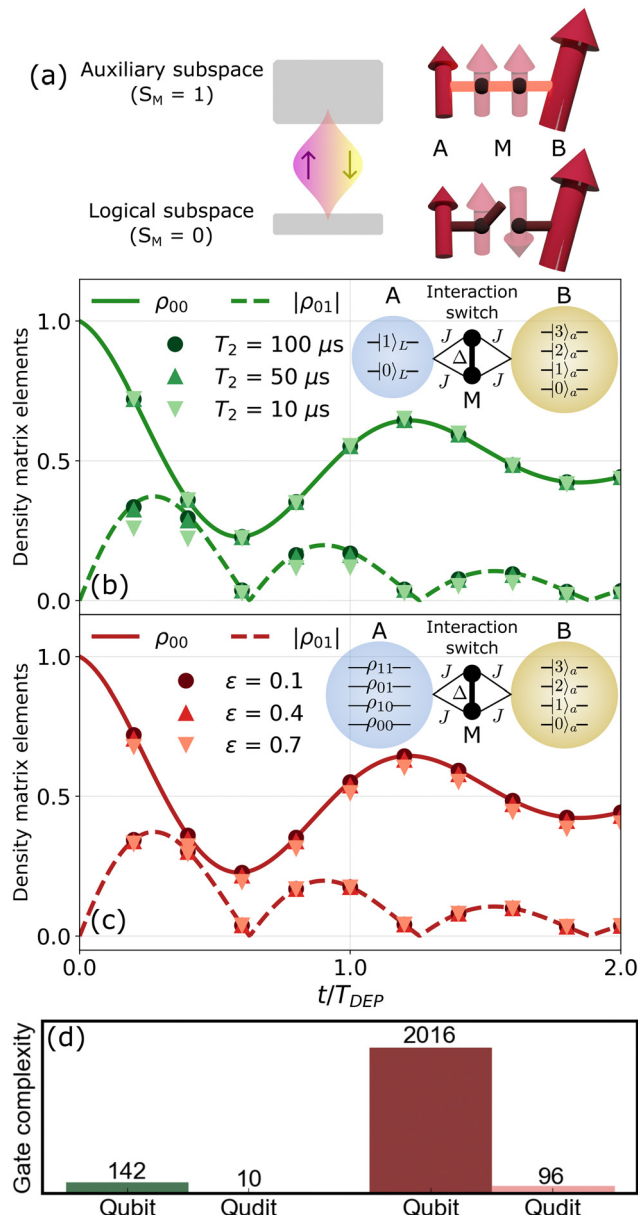

Fig. 2 (a) Scheme of how the intermediate antiferromagnetic dimer operates as an interaction switch. The A and B units only interact with each other when the M dimer is in its $S_M = 1$ excited state. (b) Dynamics of the density matrix elements of a spin-1/2 particle coupled to a depolarizing bath, simulated with the algorithm depicted in Fig. 1(b), for different natural dephasing times T_2. (c) Dynamics of the density matrix elements of a spin-1/2 particle coupled to a depolarizing bath, simulated with the algorithm depicted in Fig. 1(c), for different values of the expansion parameter ε in eqn (4). In both panels (b) and (c), a small inset schematically shows the molecular complex proposed for each algorithm. (d) Gate complexity required for the implementation of the same quantum simulation between a molecular qudit-based and a superconducting qubit-based platform for both algorithms (green bars correspond to panel (b) and red bars correspond to panel (c)).

the Cu_2 dimer and between the computational and switch units is parameterized by Δ and J, respectively. We consider a regime in which $\Delta > 0$ is much larger than both $|g_z^A - g_z^B|\mu_B B_0$ and J, such that the eigenstates of the switch are factorized from those

of the computational units A and B. The former practically correspond to a ground state singlet and an excited triplet (split by the Zeeman interaction with the external field), and the latter to the eigenstates of S_z^A ($|m_A\rangle$) and S_z^B ($|m_B\rangle$). To fulfill these conditions, we consider $\Delta/2\pi = 30$ GHz, $J/2\pi = 0.2$ GHz, and $B_0 = 700$ mT. We also assume a difference in the component of the g-factors along the direction of the microwave pulses $\Delta g_{Cu,x} = 0.2$, as could be obtained with orthogonal orientations of Cu^{2+}, while $g_z^M = 2.1$. Note the value for $\Delta/2\pi$ was chosen to keep the pulses needed to implement two-qudit gates in the microwave regime, although it can be considered rather small for some experimental realizations of the Cu_2 dimer.[66] With this choice, we define the computational subspace within the singlet ground state of the switch. As long as the switch is frozen in this subspace, the two units A and B are effectively decoupled. Then, entangling gates between A and B can be performed simply by exciting a transition of the dimer M conditioned on the states of the other spins. A basic scheme of this process is shown in Fig. 2(a). The idea is to apply two consecutive π pulses between the logic subspace (corresponding to the ground state of the dimer with $S_M = 0$) and the auxiliary subspace (excited state of the dimer with $S_M = 1$) for only a specific state of A and B. This generates entanglement between the A and B units equivalent to the application of a $C\varphi$ gate (see ref. 43 and the ESI† for details). The phase φ is controlled by the phase difference between the two pulses.

For the projective measurements required on the ancilla, we consider the coupling of the molecular complex to a superconducting resonator, described by $H_r = \omega_r a^\dagger a$, with $a^\dagger$ (a) being the bosonic creation (annihilation) operator for the photons and ω_r its resonant frequency. The full Hamiltonian that accounts for the physical hardware reads

$$H = H_{MOL} + H_r + 2G(a + a^\dagger)\sum_{\alpha=A,B} S_x^\alpha. \tag{8}$$

The last term in eqn (8) accounts for the coupling between the two molecules acting as registers in the algorithm and the resonator. The origin of this coupling lies in the Zeeman effect between the magnetic field generated by the resonator (assuming its relevant component is along the X-axis, perpendicular to the quantization axis Z) and the angular momentum of each spin. The bare coupling G is expected to reach values up to $G = 100$ kHz making use of nanoconstrictions in the inductor line in order to confine and increase the photon magnetic field,[75,76] whereas the effective coupling (including the matrix element of the spin excitation) can be further enhanced with molecular engineering to take advantage of high spin systems.[45]

Projective measurements are conducted by bringing the resonator (initialized in its vacuum state with no photons) into resonance with a transition of the molecule and detecting a possible photon emission. The emission of a photon indicates that the system was in the excited state of the corresponding transition.[45] Photons can also be exploited to mediate the interaction between distant molecules, thus implementing switchable qubit–qubit entangling gates and hence granting scalability. In particular, an efficient implementation of the

molecular-spin quantum processor focused in the simulation of OQS includes local units composed by a system and an environment qudit, whose interaction can be rapidly turned on and off by an interposed molecular switch (such as the dimer). The effective coupling between these units is then mediated by the resonator (see the simulations discussed below).

Fig. 2(a) shows the results of the simulations made for this implementation. These are obtained by numerically integrating the Lindblad equation for the hardware density matrix (see the ESI†), including the sequence of pulses needed to implement the gates, as well as the main sources of errors. These are represented by pure dephasing of the molecular spins, parameterized by time T_2, and photon loss of the resonator, with a rate of $\omega_r/2\pi Q$, with Q being the quality factor of the resonator. We plot the evolution of the ground state population, ρ_{00}, as well as the coherence, $|\rho_{01}|$, of the two-level system as a function of the relative time t/T_{DEP} for different values of the natural decoherence time of the molecules, T_2. The total pulse sequence lasts between 1.8 μs ($t/T_{DEP} = 0.25$) and 2.58 μs ($t/T_{DEP} = 2.0$), and hence even a short $T_2 = 10$ μs gives reliable results. Note that in this particular example, due to the symmetry of the problem, $N_T = 1$ suffices to exactly reproduce the joint dynamics. As can be seen from Fig. 2(c), even in the simpler case of simulating the dynamics of a spin-1/2, the reduction in gate complexity compared to a qubit-based architecture remains significant. For a 3-superconducting-qubit circuit, the application of 142 ± 4 native operations (RZ, SX, X, CNOT) is required, according to Qiskit's transpiler at its highest optimization level.[77] In contrast, our proposed platform allows the implementation of the exact same dynamics with just 10 microwave pulses (see the ESI†).

We now demonstrate the versatility offered by the molecular design with the implementation of the second algorithm presented in the previous section, shown in Fig. 1(c). Once again, we consider the dynamics of a single-qubit Hamiltonian, $\mathscr{H} = \frac{\Omega}{2}\sigma_x$, under the effect of a DEP channel. To implement both the degrees of freedom of the target system's density matrix and the auxiliary ancilla, we use two ququarts. Consequently, we opted to utilize the same molecular hardware described by Hamiltonian (7), where the spin-1/2 of unit A is replaced by another spin-3/2. The only parameters that differ from the previous implementation are $g_z^A = 1.96$, $g_z^B = 2.00$, $B_0 = 600$ mT, $D_A/2\pi = 3$ GHz, and $D_B/2\pi = 5.2$ GHz. In Fig. 2(b), we show the results for the simulated dynamics as a function of different values for the ε parameter. This parameter has important consequences for the physical implementation of the algorithm. On the one hand, a large ε value leads to an erroneous approximation. On the other hand, small values of ε require a high precision in the readout, because the final state populations have to be re-scaled by a factor $1/2\varepsilon$ [cf. eqn (4) and the ESI† for more details]. For that reason, in order to assess the resilience of the algorithm to different values of ε, we have not considered the presence of decoherence in the molecules for these simulations ($T_2 \to \infty$). Remarkably, we find that the validity of the approximation for the $e^{\mathscr{L}t}$ operator remains acceptable up to values of $\varepsilon = 0.4$.

Although the scaling in the ancilla register for this algorithm is favorable compared to the other shown in Fig. 1(b), the main bottleneck lies in the implementation of the S_m, S_p, A_m and A_p unitaries. To implement the 2-ququart gates, we have followed the decomposition algorithm of ref. 61, making use of the natural controlled-Rz gate implemented in our hardware (see the ESI†). The implementation of these 4 operations in our case requires a total of 96 microwave pulses, which compares very favorably with 2016 native operations for a circuit composed of 4 superconducting qubits, according to Qiskit's transpiler (see the ESI†). Additionally, 96 pulses are still sensibly less than the 142 operations required to implement the previous algorithm on a qubit-based quantum simulator (Fig. 2(c)). Although this method requires almost ten times more pulses than the other to simulate the same dynamics on molecular qudits, keep in mind that here there is no need for Trotter decomposition, which could give an advantage for cases requiring a large number of Trotter steps. In contrast, this second algorithm is limited by scalability. Indeed, to simulate the dynamics of N particles with spin S, we would need to implement 4 unitary operations acting on the entire d_s^2-dimensional Hilbert space conditioned by the state of the ancilla ququart, being $d_s = (2S + 1)^N$. This could introduce a significant overhead in the number of operations, despite having a smaller ancilla dimension, since it requires an all-to-all connectivity between the units of the circuit. Still, since the size $4d_s^2$ of the whole needed space rapidly grows with the size d_s of the target system, this method greatly benefits by incorporating additional levels through molecular qudits.

At this point, it should be emphasized that there are simpler molecular complexes which could substitute the proposed qudit–dimer–qudit structure at the expense of more complex pulse sequences. For instance, replacing the dimer with a single spin would result in a less efficient switch (leading to a residual second-order qudit–qudit coupling even when the switch is "off") but simpler on the synthetic side, with examples already available.[78] On the other hand, there are other schemes exploiting a different type of switch, such as a redox-active unit that can change its spin state upon oxidation.[79] Finally, the simplest option from a chemical synthesis point of view would be that of molecular nanomagnets consisting of permanently coupled A–B dimers (i.e., without the interposed switch). This structure could already fit the proposed implementation for both algorithms. For the present scheme, in which scalability of the register is ensured by coupling individual units with resonators, this would only require $\approx$ 2–4 times more parallel pulses for single qudit gates, whereas A–B entangling gates would reduce to a single pulse.[80] As a result, no significant change is expected in the overall duration of the circuit. Suitable spin qudit dimers already exist,[81–83] thus bringing our scheme closer to an experimental implementation.

2.3 Scaling

To conclude, we simulate the dynamics of a dimer composed of two interacting spin-1/2 particles, each coupled to a DEP channel, demonstrating the favourable scaling to higher-dimensionality problems of our platform based on molecular spin qudits coupled to superconducting resonators. The interaction considered follows the transverse-field Ising (TFI) model, described by the target Hamiltonian

$$\mathcal{H} = Js_z^1 s_z^2 + h_x(s_x^1 + s_x^2), \qquad (9)$$

where each s_α^i ($\alpha = x, z$, $i = 1, 2$) represents the corresponding 1/2-spin operator. In Fig. 3(a), we show a scheme of the hardware for the proposed quantum simulator. Each spin coupled to its environment would be encoded in an A_i–dimer–B_i complex (as detailed above), while the interaction between different units is mediated by the resonator. The entanglement between units A_1 and A_2 is generated by the protocol described in ref. 45, where resonant photon absorption and emission is employed to implement a controlled phase gate (see the ESI†). To address the different resonance frequencies required by this protocol, we tune the resonator's resonance frequency through SQUID loops,[45] as shown in Fig. 3(a). The quantum circuit describing the implementation of the algorithm, shown in Fig. 3(b), consists of N_T Trotter steps, each including both coherent and incoherent evolutions. Each block of gates used to simulate incoherent dynamics (grouped in U_{DEP}) is the same as the one presented in Fig. 1(b), while the coherent part is described by the sequence of unitaries $U_{zz} = e^{-iJs_z^1 s_z^2 t}$ and $U_x = e^{-ih_x s_x t}$.

Fig. 3(c.1–4) show the results obtained for several values of the different parameters. The Hamiltonian parameters J and h_x have been set to $J = -2h_x$, $h_x = 1$ (where the Trotter approximation is more critical). Moreover, to show the validity of the proposed physical implementation, both the molecular decoherence time T_2 and the resonator quality factor Q have been fixed to values compatible with real devices [cf. ref. 45]. Finally, results are presented for two different intensity regimes of the DEP channel. Panels (c.1) and (c.3) illustrate the dynamics of the total magnetization, $\langle s_z^1 + s_z^2 \rangle$, and the correlation function, $\langle s_z^1 s_z^2 \rangle$, over a characteristic time of $T_{DEP} = 15$. In contrast, panels (c.2) and (c.4) show the behavior of the same observables at $T_{DEP} = 5$, reflecting a stronger interaction between the system and the environment. We note that satisfactory results are obtained from $T_2 \geq 50$ μs and $Q \geq 10^6$. A more exhaustive analysis of the effect of noise on our simulations is reported in Fig. 3(d). We studied the fidelity $\mathscr{F}$ between the density matrices produced by our protocol, ρ_{sim}, and that expected by the exact Trotter evolution (black solid lines in panels (c.1–4) of Fig. 3), ρ_{th}, for $h_x t = 2.5$ (gray line in panels (c.1) and (c.3) of Fig. 3) and $T_{DEP} = 15$. This metric is defined as

$$\mathscr{F} = \left(\text{Tr} \sqrt{\sqrt{\rho_{sim}} \rho_{th} \sqrt{\rho_{sim}}} \right)^2, \qquad (10)$$

with $0 \leq \mathscr{F} \leq 1$.[84] The dependence of $\mathscr{F}$ on T_2 and Q is shown in Fig. 3(d). We note that T_2 limits much more than Q the maximum fidelity attainable, but reasonable values of both parameters ensure a good fidelity. It can be seen that for $T_2 > 40$ μs and $Q > 2 \times 10^5$ a fidelity higher than 0.95 is systematically obtained. We finally note that the effective spin–photon coupling considered for the simulations presented in Fig. 3(c) and (d) is 1 MHz. This can be achieved[34,45] starting
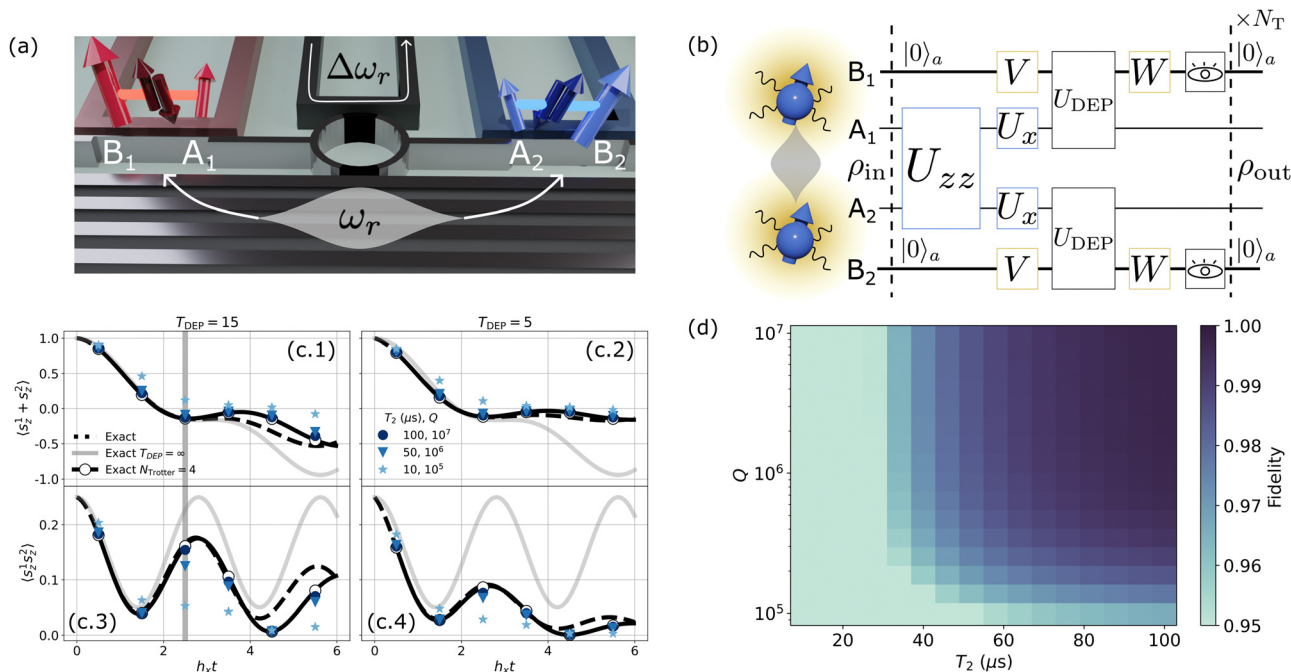
Fig. 3 (a) Schematic design of the physical hardware to simulate the dynamics of two spins A_1 and A_2 coupled to artificial environments B_1 and B_2. The resonator, characterized by a bare frequency ω_r, enables entanglement between units A_1 and A_2, as well as performing projective measurements on ancillas B_1 and B_2. The SQUID loop allows for shifts $\Delta\omega_r$ in the bare ω_r to address the different excitation frequencies required. (b) Quantum circuit to simulate the transverse field Ising model in the presence of a DEP channel for two 1/2-spins. (c) Simulation results for different characteristic times of the DEP channel and decoherence times of the molecular hardware. The time evolution for the total magnetization is shown in (c.1) and (c.2) and that of the two-body correlator in (c.3) and (c.4). Different lines show the numerical solutions considering the Trotter decomposition (black line with open dots), absence of the environment (grey solid line) and exact solution of the joint dynamics (dashed line). Different markers represent different decoherence times T_2 and resonator quality factors Q. The gray vertical line in panels (c.1) and (c.3) indicates the operating point for which the fidelity in the next panel has been calculated. (d) Fidelity $\mathscr{F}$ calculated using eqn (10) between the density matrix obtained after our pulse sequence and the expected one after the exact Trotter evolution for $h_x t = 2.5$ and $T_{DEP} = 15$, plotted as a function of T_2 and Q.

from a bare coupling of 100 kHz and encoding of the two logical levels needed for the spin-1/2 target particle in the two lowest $|m|$ states of an $S = 10$ molecule (such as Fe_8 or Mn_{12}), which would provide a further enhancement of one order of magnitude.

As a last note, we estimate that the simulation of these same dynamics using the second algorithm would result in a pulse sequence incompatible with the available decoherence rates and photon loss in our experimental platform, as well as beyond the computational resources at our current reach.

3 Conclusion

In summary, we have investigated two conceptually distinct algorithms that align with the current state of the art in the field and extended them to a qudit-based architecture. In this context, it has been analyzed how, in the current era of noisy devices, algorithms that prioritize the use of additional units in exchange for shallower circuits (as in Fig. 1(b)) may be more advantageous. This is in contrast to more sophisticated algorithms that require deeper circuits (as in Fig. 1(c)), which often exceed the available coherence times in current systems but will become crucial in the fault-tolerant era. We have demonstrated that the use of systems with $d > 2$ levels largely narrows the gap

between circuit execution times and system decoherence times. This is achieved by reducing the number of required operations to be implemented in all considered cases, reaching a reduction of almost two orders of magnitude in some scenarios. To this end, we have shown through realistic simulations that molecular spin qudits are ideal candidates for the implementation of qudit-based codes due to their natural ability to host many accessible levels and their chemical engineerability. In Section 2.2, we have shown that even the simulation of a simple spin-1/2 OQS can benefit greatly from the use of qudits, reducing the gate complexity by a factor of 10. Moreover, with execution times of less than 3 μs, we consider that the first experimental proofs of concept could be realized in the near future. Furthermore, in Section 2.3, we have explored the next steps to be taken in order to simulate more than a single particle by exploiting the scalability offered by superconducting circuits. Through detailed simulations (see Fig. 3(d)), we have shown that the prevailing noise levels needed to obtain satisfactory results even for these advanced quantum circuits are not beyond the scope of what should be expected in the near future for these platforms (spin decoherence times $T_2 > 40$ μs and photon loss through the resonator quality factor $Q > 2 \times 10^5$).[45] However, work still lies ahead to find compounds that meet the coherence and control requirements outlined in this work.

Nonetheless, the results regarding the reduction of the gate complexity presented in this work are applicable to any platform capable of implementing and coherently controlling systems with more than two levels. Similarly, we consider that the use of qudits can be beneficial for any OQS simulation algorithm, such as the one presented in ref. 23, where the ancilla grows with the number of jump operators, or the Sz.-Nagy algorithm,[22,30] where the action of each Kraus operator is simulated in parallel and combined classically in the post-processing. In the latter case, although the required ancilla is a single two-level system, the use of qudits can reduce the number of non-local operations to be implemented by using fewer units to store the same amount of logical levels.

As a final note, we believe that this work serves as a call to join efforts between the physics and the materials science community towards the design of devices that allow for the implementation of advanced quantum algorithms to efficiently study crucial phenomena such as the dynamics of open quantum systems.

Author contributions

Conceptualization: A. C. and S. C.; methodology: S. R.-J., E. M. and A. C.; investigation: S. R.-J. and E. M.; software: S. R.-J.; writing – original draft: S. R.-J. and E. M.; writing – review and editing: A. C., P. S. and S. C.; supervision: P. S. and S. C.; funding acquisition: S. C.; project administration: S. C.

Data availability

All the data shown in the figures of the article are available on Zenodo at DOI: **https://doi.org/10.5281/zenodo.14833902**.

Conflicts of interest

There are no conflicts to declare.

Acknowledgements

Notes and references

1 J. Preskill, *Quantum*, 2018, **2**, 79.

2 R. P. Feynman, *Int. J. Theor. Phys.*, 1982, **21**, 467–488.

3 F. Arute, *et al.*, *Nature*, 2019, **574**, 505.

4 S. Lloyd, *Science*, 1996, **273**, 1073–1078.

5 D. Bacon, A. M. Childs, I. L. Chuang, J. Kempe, D. W. Leung and X. Zhou, *Phys. Rev. A:At., Mol., Opt. Phys.*, 2001, **64**, 062302.

6 S. Lloyd and L. Viola, *Phys. Rev. A:At., Mol., Opt. Phys.*, 2001, **65**, 010101.

7 L. Gui-Lu, *Commun. Theor. Phys.*, 2006, **45**, 825.

8 E. Andersson and D. K. L. Oi, *Phys. Rev. A:At., Mol., Opt. Phys.*, 2008, **77**, 052104.

9 M. Kliesch, T. Barthel, C. Gogolin, M. Kastoryano and J. Eisert, *Phys. Rev. Lett.*, 2011, **107**, 120501.

10 H. Wang, S. Ashhab and F. Nori, *Phys. Rev. A:At., Mol., Opt. Phys.*, 2011, **83**, 062317.

11 R. Sweke, I. Sinayskiy, D. Bernard and F. Petruccione, *Phys. Rev. A:At., Mol., Opt. Phys.*, 2015, **91**, 062308.

12 A. Chenu, M. Beau, J. Cao and A. del Campo, *Phys. Rev. Lett.*, 2017, **118**, 140403.

13 R. Cleve and C. Wang, 44th International Colloquium on Automata, Languages, and Programming (ICALP 2017), Dagstuhl, Germany, 2017, pp. 17:1–17:14.

14 R. Iten, R. Colbeck and M. Christandl, *Phys. Rev. A*, 2017, **95**, 052316.

15 F. Ticozzi and L. Viola, *Quantum Sci. Technol.*, 2017, **2**, 034001.

16 J. T. Barreiro, M. Müller, P. Schindler, D. Nigg, T. Monz, M. Chwalla, M. Hennrich, C. F. Roos, P. Zoller and R. Blatt, *Nature*, 2011, **470**, 486–491.

17 H. Lu, C. Liu, D.-S. Wang, L.-K. Chen, Z.-D. Li, X.-C. Yao, L. Li, N.-L. Liu, C.-Z. Peng, B. C. Sanders, Y.-A. Chen and J.-W. Pan, *Phys. Rev. A*, 2017, **95**, 042310.

18 C. Shen, K. Noh, V. V. Albert, S. Krastanov, M. H. Devoret, R. J. Schoelkopf, S. M. Girvin and L. Jiang, *Phys. Rev. B*, 2017, **95**, 134501.

19 T. Xin, S. J. Wei, J. S. Pedernales, E. Solano and G. L. Long, *Phys. Rev. A*, 2017, **96**, 022302.

20 L. Hu, X. Mu, W. Cai, Y. Ma, Y. Xu, H. Wang, Y. Song, C. L. Zou and L. Sun, *Sci. Bull.*, 2018, **63**, 1551–1557.

21 J. Han, W. Cai, L. Hu, X. Mu, Y. Ma, Y. Xu, W. Wang, H. Wang, Y. P. Song, C. L. Zou and L. Sun, *Phys. Rev. Lett.*, 2021, **127**, 020504.

22 A. Gaikwad, Arvind and K. Dorai, *Phys. Rev. A*, 2022, **106**, 022424.

23 M. Cattaneo, M. A. Rossi, G. García-Pérez, R. Zambrini and S. Maniscalco, *PRX Quantum*, 2023, **4**, 010324.

24 W. F. Stinespring, *Proc. Am. Math. Soc.*, 1955, **6**, 211–216.

25 H. Kamakari, S. N. Sun, M. Motta and A. J. Minnich, *PRX Quantum*, 2022, **3**, 010320.

26 Z. Hu, R. Xia and S. Kais, *Sci. Rep.*, 2020, **10**, 3301.

27 A. W. Schlimgen, K. Head-Marsden, L. M. Sager, P. Narang and D. A. Mazziotti, *Phys. Rev. Lett.*, 2021, **127**, 270503.

28 A. W. Schlimgen, K. Head-Marsden, L. A. M. Sager-Smith, P. Narang and D. A. Mazziotti, *Phys. Rev. A*, 2022, **106**, 022414.

29 A. W. Schlimgen, K. Head-Marsden, L. A. M. Sager, P. Narang and D. A. Mazziotti, *Phys. Rev. Res.*, 2022, **4**, 023216.

30 N. Suri, J. Barreto, S. Hadfield, N. Wiebe, F. Wudarski and J. Marshall, *Quantum*, 2023, **7**, 1002.

31 Y. Wang, E. Mulvihill, Z. Hu, N. Lyu, S. Shivpuje, Y. Liu, M. B. Soley, E. Geva, V. S. Batista and S. Kais, *J. Chem. Theory Comput.*, 2023, **19**, 4851–4862.

32 W. Cai, J. Han, L. Hu, Y. Ma, X. Mu, W. Wang, Y. Xu, Z. Hua, H. Wang, Y. P. Song, J.-N. Zhang, C.-L. Zou and L. Sun, *Phys. Rev. Lett.*, 2021, **127**, 090504.

33 S. Carretta, D. Zueco, A. Chiesa, A. Gómez-León and F. Luis, *Appl. Phys. Lett.*, 2021, **118**, 240501.

34 A. Chiesa, P. Santini, E. Garlatti, F. Luis and S. Carretta, *Rep. Prog. Phys.*, 2024, **87**, 034501.

35 J. M. Zadrozny, J. Niklas, O. G. Poluektov and D. E. Freedman, *ACS Cent. Sci.*, 2015, **1**, 488–492.

36 K. Bader, M. Winkler and J. van Slageren, *Chem. Commun.*, 2016, 3623–3626.

37 M. Atzori, L. Tesi, E. Morra, M. Chiesa, L. Sorace and R. Sessoli, *J. Am. Chem. Soc.*, 2016, **138**, 2154–2157.

38 M. Atzori, E. Morra, L. Tesi, A. Albino, M. Chiesa, L. Sorace and R. Sessoli, *J. Am. Chem. Soc.*, 2016, **138**, 11234–11244.

39 M. Atzori, L. Tesi, S. Benci, A. Lunghi, R. Righini, A. Taschin, R. Torre, L. Sorace and R. Sessoli, *J. Am. Chem. Soc.*, 2017, **139**, 4338–4341.

40 D. Aguilà, D. Barrios, V. Velasco, O. Roubeau, A. Repollés, P. Alonso, J. Sesé, S. Teat, F. Luis and G. Aromí, *J. Am. Chem. Soc.*, 2014, **136**, 14215.

41 A. Ardavan, A. M. Bowen, A. Fernandez, A. J. Fielding, D. Kaminski, F. Moro, C. A. Muryn, M. D. Wise, A. Ruggi, E. J. L. McInnes, K. Severin, G. A. Timco, C. R. Timmel, F. Tuna, G. F. S. Whitehead and R. E. P. Winpenny, *npj Quantum Inf.*, 2015, **1**, 15012.

42 J. Ferrando-Soria, E. Moreno-Pineda, A. Chiesa, A. Fernandez, S. A. Magee, S. Carretta, P. Santini, I. Vitorica-Yrezabal, F. Tuna, E. J. L. McInness and R. E. P. Winpenny, *Nat. Commun.*, 2016, **7**, 11377.

43 P. Santini, S. Carretta, F. Troiani and G. Amoretti, *Phys. Rev. Lett.*, 2011, **107**, 230502.

44 C. J. Wedge, G. A. Timco, E. T. Spielberg, R. E. George, F. Tuna, S. Rigby, E. J. L. McInnes, R. E. P. Winpenny, S. J. Blundell and A. Ardavan, *Phys. Rev. Lett.*, 2012, **108**, 107204.

45 A. Chiesa, S. Roca, S. Chicco, M. de Ory, A. Gómez-León, A. Gomez, D. Zueco, F. Luis and S. Carretta, *Phys. Rev. Appl.*, 2023, **19**, 064060.

46 A. Urtizberea, E. Natividad, P. J. Alonso, L. Pérez-Martínez, M. A. Andrés, I. Gascón, I. Gimeno, F. Luis and O. Roubeau, *Mater. Horiz.*, 2020, **7**, 885–897.

47 A. Ghirri, C. Bonizzoni, F. Troiani, N. Buccheri, L. Beverina, A. Cassinese and M. Affronte, *Phys. Rev. A*, 2016, **93**, 063855.

48 S. Carretta, A. Chiesa, F. Troiani, D. Gerace, G. Amoretti and P. Santini, *Phys. Rev. Lett.*, 2013, **111**, 110501.

49 A. Chiesa, P. Santini, D. Gerace, J. Raftery, A. A. Houck and S. Carretta, *Sci. Rep.*, 2015, **5**, 16036.

50 A. Chiesa, E. Macaluso, F. Petiziol, S. Wimberger, P. Santini and S. Carretta, *J. Phys. Chem. Lett.*, 2020, **11**, 8610–8615.

51 M. Chizzini, L. Crippa, L. Zaccardi, E. Macaluso, S. Carretta, A. Chiesa and P. Santini, *Phys. Chem. Chem. Phys.*, 2022, **24**, 20030.

52 M. Mezzadri, A. Chiesa, L. Lepori and S. Carretta, *Mater. Horiz.*, 2024, **11**, 4961–4969.

53 F. Tacchino, A. Chiesa, R. Sessoli, I. Tavernelli and S. Carretta, *J. Mater. Chem. C*, 2021, **9**, 10266–10275.

54 S. Chicco, G. Allodi, A. Chiesa, E. Garlatti, C. D. Buch, P. Santini, R. De Renzi, S. Piligkos and S. Carretta, *J. Am. Chem. Soc.*, 2024, **146**, 1053–1061.

55 M. A. Nielsen, M. R. Dowling, M. Gu and A. C. Doherty, *Science*, 2006, **311**, 1133–1135.

56 S. Roca-Jerat, T. Sancho-Lorente, J. Román-Roche and D. Zueco, *SciPost Phys.*, 2023, **15**, 186.

57 T. F. Havel, *J. Math. Phys.*, 2003, **44**, 534–557.

58 H.-P. Breuer and F. Petruccione, *The theory of open quantum systems*, Oxford University Press, USA, 2002.

59 D. Tupkary, A. Dhar, M. Kulkarni and A. Purkayastha, *Phys. Rev. A*, 2022, **105**, 032208.

60 N. Hatano and M. Suzuki, *Finding Exponential Product Formulas of Higher Orders*, Springer, Berlin, Heidelberg, 2005, pp. 37–68.

61 L. E. Fischer, A. Chiesa, F. Tacchino, D. J. Egger, S. Carretta and I. Tavernelli, *PRX Quantum*, 2023, **4**, 030327.

62 M. Ringbauer, M. Meth, L. Postler, R. Stricker, R. Blatt, P. Schindler and T. Monz, *Nat. Phys.*, 2022, **18**, 1053–1057.

63 P. Hrmo, B. Wilhelm, L. Gerster, M. W. van Mourik, M. Huber, R. Blatt, P. Schindler, T. Monz and M. Ringbauer, *Nat. Commun.*, 2023, **14**, 2242.

64 I. Gimeno, A. Urtizberea, J. Román-Roche, D. Zueco, A. Camón, P. J. Alonso, O. Roubeau and F. Luis, *Chem. Sci.*, 2021, **12**, 5621–5630.

65 M. Atzori and R. Sessoli, *J. Am. Chem. Soc.*, 2019, **141**, 11339–11352.

66 G. A. Timco, S. Carretta, F. Troiani, F. Tuna, R. J. Pritchard, C. A. Muryn, E. J. L. McInnes, A. Ghirri, A. Candini, P. Santini, G. Amoretti, M. Affronte and R. E. P. Winpenny, *Nat. Nanotechnol.*, 2009, **4**, 173–178.

67 S. J. Lockyer, A. Chiesa, A. Brookfield, G. A. Timco, G. F. S. Whitehead, E. J. L. McInnes, S. Carretta and R. E. P. Winpenny, *J. Am. Chem. Soc.*, 2022, **144**, 16086–16092.

68 M. J. Graham, J. M. Zadrozny, M. Shiddiq, J. S. Anderson, M. S. Fataftah, S. Hill and D. E. Freedman, *J. Am. Chem. Soc.*, 2014, **136**, 7623–7626.

69 V. Rollano, M. C. de Ory, C. D. Buch, M. Rubn-Osanz, D. Zueco, C. Sánchez-Azqueta, A. Chiesa, D. Granados, S. Carretta, A. Gomez, S. Piligkos and F. Luis, *Commun. Phys.*, 2022, **5**, 246.

70 S. Thiele, F. Balestro, R. Ballou, S. Klyatskaya, M. Ruben and W. Wernsdorfer, *Science*, 2014, **344**, 1135–1138.

71 M. Atzori, A. Chiesa, E. Morra, M. Chiesa, L. Sorace, S. Carretta and R. Sessoli, *Chem. Sci.*, 2018, **9**, 6183.

72 D. Ranieri, F. Santanni, A. Privitera, A. Albino, E. Salvadori, M. Chiesa, F. Totti, L. Sorace and R. Sessoli, *Chem. Sci.*, 2023, **14**, 61–69.

73 A. Abragam and B. Bleaney, *Electron paramagnetic resonance of transition ions*, OUP, Oxford, 2012.

74 P. C. E. Stamp and I. S. Tupitsyn, *Phys. Rev. B:Condens. Matter Mater. Phys.*, 2004, **69**, 014401.

75 M. D. Jenkins, U. Naether, M. Ciria, J. Sesé, J. Atkinson, C. Sánchez-Azqueta, E. D. Barco, J. Majer, D. Zueco and F. Luis, *Appl. Phys. Lett.*, 2014, **105**, 162601.

76 I. Gimeno, W. Kersten, M. C. Pallarés, P. Hermosilla, M. J. Martnez-Pérez, M. D. Jenkins, A. Angerer, C. Sánchez-Azqueta, D. Zueco, J. Majer, A. Lostao and F. Luis, *ACS Nano*, 2020, **14**, 8707–8715.

77 Qiskit contributors, *Qiskit: An Open-source Framework for Quantum Computing*, 2023.

78 A. Chiesa, G. F. S. Whitehead, S. Carretta, L. Carthy, G. A. Timco, S. J. Teat, G. Amoretti, E. Pavarini, R. E. P. Winpenny and P. Santini, *Sci. Rep.*, 2014, **4**, 7423.

79 J. Lehmann, A. Gaita-Arino, E. Coronado and D. Loss, *Nat. Nanotechnol.*, 2007, **2**, 312–317.

80 F. Luis, A. Repollés, M. J. Martínez-Pérez, D. Aguilà, O. Roubeau, D. Zueco, P. J. Alonso, M. Evangelisti, A. Camón, J. Sesé, L. A. Barrios and G. Aromí, *Phys. Rev. Lett.*, 2011, **107**, 117203.

81 T. Sanada, T. Suzuki, T. Yoshida and S. Kaizaki, *Inorg. Chem.*, 1998, **37**, 4712–4717.

82 F. Luis, P. J. Alonso, O. Roubeau, V. Velasco, D. Zueco, D. Aguilà, J. I. Martínez, L. A. Barrios and G. Aromí, *Commun. Chem.*, 2020, **3**, 176.

83 H. Biard, E. Moreno-Pineda, M. Ruben, E. Bonet, W. Wernsdorfer and F. Balestro, *Nat. Commun.*, 2021, **12**, 4443.

84 M. A. Nielsen and I. L. Chuang, *Quantum computation and quantum information*, Cambridge University Press, 2010.